

Ultrafast photoelimination of nitrogen from upper excited states of diazoalkanes and the fate of carbenes formed in the reaction

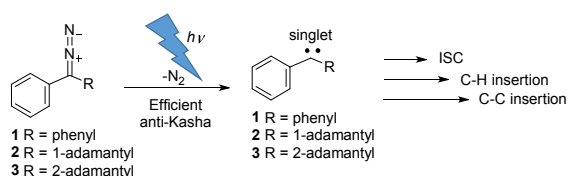
Vedran Brusar,[‡] Mateo Forjan,[‡] Ivan Ljubić,^{§*}, Marija Alešković,[‡] Kristin Becker,[‡] Silvij
Vdović^{‡*}

[‡] Centre for Advanced Laser Techniques, Institute of Physics, Bijenička cesta 46, 10 000 Zagreb, Croatia. E-mail: silvije@ifs.hr

[§] Department of Physical Chemistry, Ruđer Bošković Institute, Bijenička cesta 54, 10 000 Zagreb, Croatia. E-mail: ivan.ljubic@irb.hr

[‡] Department of Organic Chemistry and Biochemistry, Ruđer Bošković Institute, Bijenička cesta 54, 10 000 Zagreb, Croatia.

Table of Contents



Abstract: Photochemical reactivity of diphenyldiazomethane **1**, and phenyl 1- and 2-adamantyl diazomethanes **2** and **3** was investigated experimentally by transient absorption spectroscopy (TA) with the time resolution from femtoseconds to milliseconds. We have gathered spectroscopic evidence that the photoelimination of N₂ upon excitation at 267 nm takes place in the anti-Kasha ultrafast photochemical reaction within 1 ps directly from the upper excited

singlet states. The N₂ elimination delivers singlet carbenes, that were in the case of **1** and **2** detected by fs-TA. The reactivity of carbenes differs with respect to the substituent at the carbene center. The singlet **car-1** in nonpolar solvent predominantly delivers the triplet carbene by ISC. On the contrary, ISC for **car-2** giving the corresponding triplet carbene was not detected. Instead, the singlet **car-2** has longer lifetimes and reacts in the intermolecular insertion reactions into C-H bonds. **Car-3** has an α C-H bond next to the carbene center, and therefore, reacts rapidly in the intramolecular C-H insertion reaction delivering alkene photoproduct, precluding its detection by fs-TA. However, isolation of ketone photoproducts from **3** is highly indicative of the formation of the triplet **car-3** as a reactive intermediate. The TA spectra from the S₁, S₂, and S₃ excited states of **1**, **2**, and **3** were computed using time-dependent density functional theory (TD-CAM-B3LYP) while the multiconfigurational perturbation theory to the second order (CASPT2) was used for the absorption spectra of the corresponding singlet and triplet carbenes. The modeled and measured TA spectra are in good agreement, and the computations corroborate the assignments of the key short-lived intermediates in the photoinduced reactions of **1**, **2**, and **3**.

Key words: carbenes, diazo compounds, anti-Kasha photochemistry, transient spectroscopy, density functional theory, multiconfigurational quantum chemistry

Introduction

Since the seminal papers of Hine¹ and Doering,² carbene chemistry developed into intensively investigated topic,^{3,4,5} primarily owing to the applications of stable carbenes⁶ in catalysis.^{7,8}

Moreover, significant endeavors were undertaken in the investigation of physical-organic aspects of carbene chemistry⁹ and elucidating carbene reaction mechanisms and reactivity.¹⁰ One important reaction to generate carbenes is thermally or photochemically induced elimination of nitrogen from diazoalkanes,¹¹ which can also be used in biological systems.^{12,13} Diazoalkanes are versatile reagents in organic synthesis.¹⁴ Thus, diazomethane has been known for more than a century and used in the methylation of carboxylic acids, alcohols, phenols, cyclopropanations, ring expansions and cycloadditions.¹⁵ Moreover, the use of diazo compounds has been demonstrated in stereoselective synthesis,¹⁶ or in the complexation with transition metals and catalysis.^{17,18}

The photochemical reaction mechanism for elimination of nitrogen from diazoalkanes has been investigated by several groups.^{19, 20, 21} Moreover, Piteša et al. have recently shown that elimination of nitrogen takes place more efficiently upon excitation to higher singlet excited states in the anti-Kasha photochemical reactions.²² **Anti-Kasha photochemical reactivity has also been demonstrated in the photoelimination of nitrogen from the Meldrum's acid whereupon ketenes are formed in the Wolff rearrangement.**²³ However, for diverse molecules some questions still remain open, such as if carbene intermediates are formed in the photoelimination of nitrogen from diazo compounds having an α -H atom with respect to the diazo group, or N_2 elimination and α C-H insertion takes place simultaneously⁴ in the rearrangements in the excited state (RIES).^{24,25,26,27,28} The RIES has been debated for the elimination of carbenes from diazirines,²⁹ as well as for diazo compounds.^{19,30}

Here we report on the investigation of carbene formation from diazo carbene precursors **1-3** (Fig. 1) by femtosecond transient absorption spectroscopy (fs-TA) and laser flash photolysis (LFP). The findings were corroborated by the computations of the transient spectra carried out in the

framework of time-dependent density functional theory and multiconfigurational perturbation theory to the second order. Our experiments provide the first direct experimental spectroscopic evidence for the carbene generation directly from the FC state in the anti-Kasha photochemical reaction. The anti-Kasha photochemistry is gaining importance as it provides new opportunities in fine-tuning of the reactivity by appropriate choice of light wavelength.³¹ Moreover, we present evidence for the carbene generation from both adamantyl precursors **2** and **3**, although the latter has α C-H bond to the carbene center.

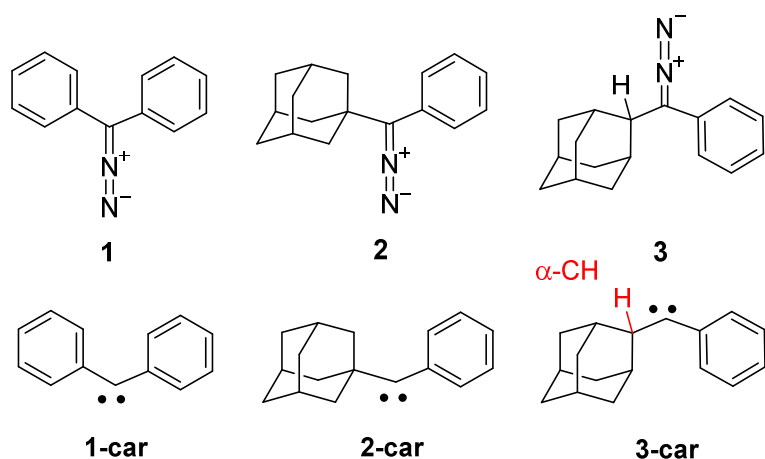


Figure 1. Investigated diazo derivatives **1-3** and the corresponding carbenes **car-1 – car-3**.

Results and discussion

Photochemical generation of carbenes from **1** and chemistry of the corresponding carbenes has been intensively investigated.^{32, 33, 34, 35, 36, 37, 38, 39, 40, 41, 42, 43} Furthermore, synthesis and photochemistry of **2** has been reported by Eguchi et al,⁴⁴ and Piteša,²² whereas **3** has hitherto never been prepared. The details on the synthesis of **1-3** are given in the experimental section and in the supporting information (Schemes S1-S3).

Ground state structures, conformations and relative energies

Fig. 2 depicts the structures of the ground state, and S_1 and T_1 minima of **1**, **2**, and **3** with the indicated relevant geometric parameters. The corresponding Cartesian coordinates and harmonic frequencies are given in Table S7. Using the CAM-B3LYP(+PCM)/6-311+G(2d,p) level, the global conformational minima of **1**, **2**, and **3** and their corresponding carbenes were found by performing the relaxed structural scans with respect to the torsion around the C–C(N₂) bonds. The energy difference between the minimum and maximum rotamer in **3** is found to be 6.3 kcal mol⁻¹, in contrast to the nearly free rotation in **1** and **2**, where these differences are only 1.6 and 1.4 kcal mol⁻¹. The minimum conformers of **1** and singlet and triplet **car-1** exhibit the C_2 point group symmetry; the similar structures were reported before.^{22,40} The conformational preferences in **1**, **2** and **3** reflect the compromise between reduction of the steric strain with respect to the two bulky substituents and enhancement of the conjugation between the C-N-N and benzene π -densities. The two opposing effects determine the optimal angles closed by the C-N-N axis and the plane of the benzene ring, which equal 29, 7, and 19° in **1**, **2**, and **3**, respectively. The vertical first ionization potentials (IP) computed at the EPT-P3+/cc-pVTZ level equal 7.416, 7.364, and 7.421 eV for **1**, **2**, and **3**, respectively. They mirror the stability of the corresponding HOMOs depicted in Fig. S15 in the SI.

Another factor that influences the conformational minima of **2** and **3** is the hyperconjugation. Here this effect concerns the stabilizing interaction of the C-N-N and benzene ring π -density with the adjacent σ (C-H) and σ (C-C) bonds of the adamantyl moiety. The HOMOs of **2** and **3** (Fig. S15) clearly show how the π -density is delocalized over these σ -bonds. By applying the energy decomposition analysis, it has been shown that σ (C-H) bond in interaction with various π -systems typically gives rise to larger orbital stabilization terms than does σ (C-C) bond.⁴⁵ This

is also the case here, and leads to the larger first IP and the more hindered rotation in **3** compared to **2** (vide supra). Likewise, the wavenumbers for the corresponding torsional motion equal 12 and 27 cm^{-1} in **2** and **3**, respectively (Table S7).

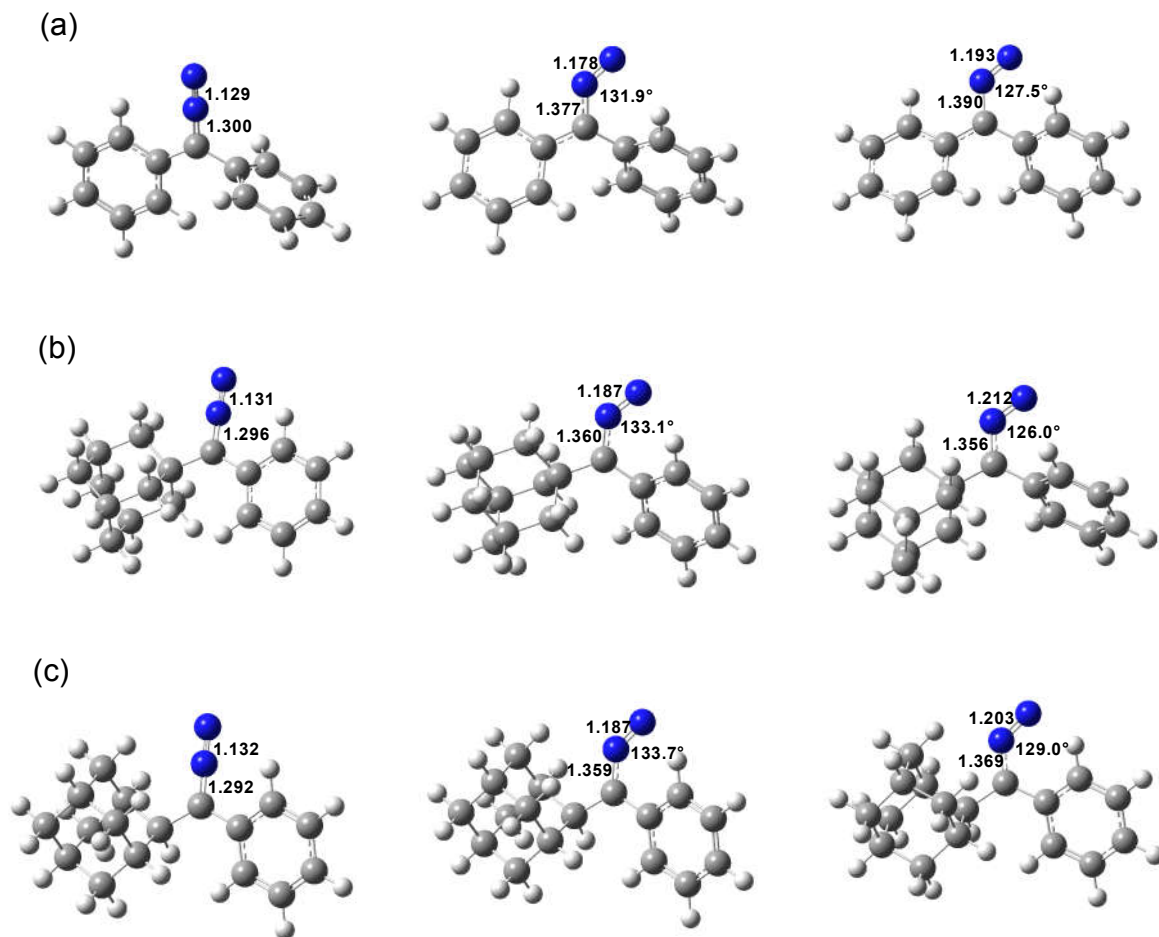


Figure 2. The C-N and N-N bond lengths (\AA), and C-N-N angles in the minimum geometries of the S_0 , S_1 and T_1 states of **1** (a), **2** (b), and **3** (c).

The triplet carbenes are in all cases predicted to be more stable than their singlet counterparts. The CAM-B3LYP(+PCM) method gives the singlet-triplet (S-T) free energy gaps (298 K) of 7.4, 9.4, and 7.3 kcal mol^{-1} for **car-1**, **car-2**, and **car-3**, respectively. The tangibly more

stabilized triplet **car-2** compared to **car-1** and **car-3** triplets is also confirmed by the CASPT2 method (0 K; ZPE not included); the gaps here are 5.3, 11.1, and 7.3 kcal mol⁻¹.

Photophysical properties

Prior to conducting photochemistry, we investigated photophysical properties of **3**, whereas photophysical properties of **1** and **2** have been disclosed.^{22,32-43} Absorption and fluorescence spectra of **3** were measured in pentane and benzene (see Figs S1-S3 in the SI). They show the same features as reported for **2**.²¹ The diazo compounds are characterized by two absorption bands. The band at ≈ 500 nm is very weak whereas that at ≈ 300 nm is very strong. The two can be correlated with the transitions to the S₁₋₃ excited states, which in the vertical TD-CAM-B3LYP spectra of **2** (**3**) are found at 479 (483), 275 (273), and 262 (263) nm carrying the respective oscillator strengths of 0.000 (0.001), 0.414 (0.409), and 0.090 (0.101). The energies of the first three vertical transitions are diagrammed in Figure 3. The full computed vertical absorption spectra are provided in Table S4. In the natural transition orbitals (NTO) picture, the relative strength of these transitions can be rationalized by the local symmetry properties of the initial and final π orbitals. Thus, transition to S₁ is weak because the involved π orbitals are mutually orthogonal (analogously to $n \rightarrow \pi^*$ transition; Fig. S16) while transition to S₂ is strong because the π orbitals are parallel (analogously to $\pi \rightarrow \pi^*$ transition; Fig. S17 in the SI). The relatively large energy gap of more than 2 eV between S₁ and S₂ for this class of compounds is in agreement with the previous results²² and is here also confirmed for **3**. In modeling the early TA spectra corresponding to the vertical (FC) geometries (vide infra), we consider the contributions of both S₂ and S₃ as in **1**, **2**, and **3** these states are separated by only 0.1 eV and the transition to S₃ is still sufficiently intense (Table S4).

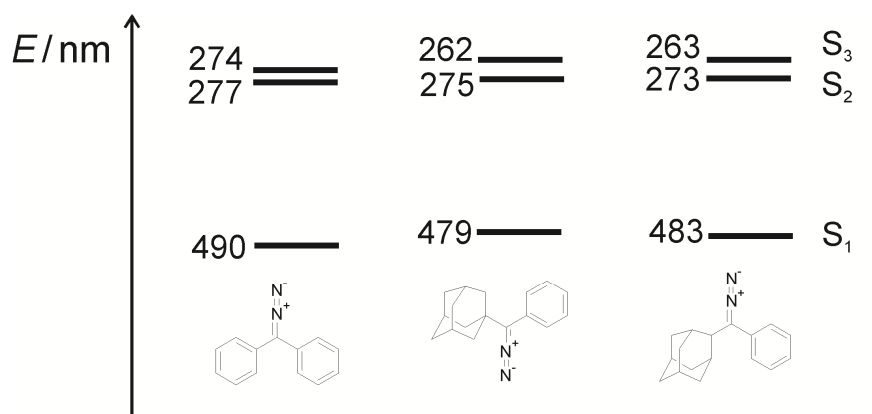


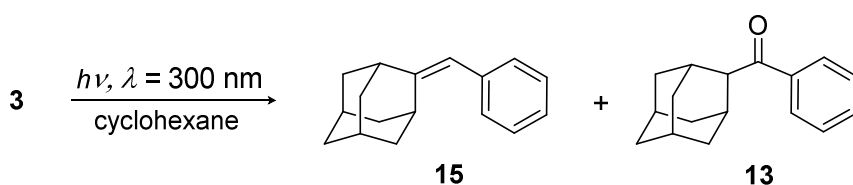
Figure 3. Energy diagram corresponding to the first three singlet excited states (S_1 , S_2 , and S_3) of **1**, **2**, and **3** computed at the TD-CAM-B3LYP(+PCM)/6-311+G(2d,p) level.

Similar to **2**, but unlike to **1**, **3** is weakly fluorescent when excited to S_n with the quantum yield of fluorescence $\Phi_F \approx 0.04$. Upon excitation to S_1 fluorescence could not be detected (Fig. S3 in the SI). The results indicate that fluorescence takes place from S_n , prior to internal conversion (IC) to S_1 . The finding can be explained by a large energy gap between S_1 and S_n which results in weak non-adiabatic coupling between these states and slow IC transitions. Decay of fluorescence for **2** and **3** in benzene was fit to bi-exponential function suggesting more complex photophysics involving at least two excited states (Table S3). Note, however, that long lifetimes of higher excited states (1.65 and 14.65 ns) are in contradiction with the observed anti-Kasha photochemical reactivity from these states that takes place in sub-picosecond time scale (*vide infra*). This inconsistency may be explained by different excited states involved in photoreaction or emission.

Photochemistry

Prompted by the observation of fluorescence for **2** and **3** from higher excited states, we investigated if these molecules show anti-Kasha photochemistry. Preparative irradiations for **2**²² and **3** were performed in cyclohexane and benzene upon excitation with visible light (cool white lamps, corresponding to the population of S_1) or at ≈ 300 nm giving rise to population of S_n (where $n > 1$).

Upon irradiation of **3** in cyclohexane, **15** was formed as the major product, resulting from the carbene insertion into the α C-H bond (Scheme 1 and Table S1). Isolation of the photoproducts was done by chromatography using 254 nm lamp. In addition, we isolated some smaller amounts of ketone **13**, formed due to the traces of dissolved oxygen in the solvent, which is a strong indication that carbene intermediate was present in the solution. It is generally known that singlet carbenes react with O_2 slowly ($k < 10^7 \text{ M}^{-1}\text{s}^{-1}$), whereas reaction of triplet carbenes with O_2 is much faster ($k = 10^8\text{-}10^{10} \text{ M}^{-1}\text{s}^{-1}$).⁵ Therefore, products from the irradiation of **3** in cyclohexane indicate formation of both, singlet and triplet carbene intermediates as reported in the photochemistry of adamantane diazirine.⁴⁶ Quantum yield for the elimination of nitrogen (Φ_R) upon excitation at 300 nm or by visible light was measured by use of ferrioxalate actinometer (for details see the SI, Table S2).^{47,48} In agreement with the photochemistry of **1** and **2**,²² Φ_R is almost an order of magnitude larger upon excitation to higher singlet excited state at 300 nm ($\Phi_R = 0.34\text{-}0.36$), then upon excitation to S_1 ($\Phi_R = 0.005\text{-}0.1$), indicating that **3** also undergoes anti-Kasha photochemistry.



Scheme 1. Photolysis of **3**.

Excited states and transient species

The strongest transitions in the vertical excited state absorption (ESA) spectra of **1**, **2**, and **3** computed at the S_0 (FC) minimum geometries are shown in Table 1. Additional strong transitions, e.g. for the transient spectra calculated at the S_1 minimum geometries, are provided in Table S5.. The ESA spectra modelled using the Gaussian broadening with the full-width-at-half-maximum parameter set to 3000 cm^{-1} are shown below (Figs 4, 6 and 8). The NTOs for the strongest ESA transitions in the FC S_1 spectra computed at the TD-CAM-B3LYP(+PCM)/ma-def2-TZVP(-f) level are depicted in Fig. S16 in the SI. Some of the excited states, which give rise to weak transitions from the S_0 ground state, can become very bright when the transition originates from S_{1-3} . It is invariably found that in case of the strongest transitions the two involved excited states have closely similar dominant particle NTOs, as it is for example observed for the $S_1 \rightarrow S_{12}$ transition in **1** (Fig. S16).

For the $S_0 \rightarrow S_1$ and $S_0 \rightarrow S_2$ transitions in **1** and **2**, the dominant NTOs obtained by the TD-CAM-B3LYP(+PCM) method (Figs. S16 and S17 in the SI) are analogous to the ADC(2)/cc-pVDZ ones.²² The character of the dominant NTOs already anticipates the anti-Kasha photochemistry; namely, why it is difficult for the C-N bond to survive the transition to S_2 . In this state the $\pi(\text{C-N})$ bonding interaction is depleted of its charge density, which is transferred towards the benzene ring(s) and/or the $\pi(\text{N-N})$ bond (Fig. S17 in the SI). Consequently, we observed that the attempts at optimizing the S_2 minimum fail when the structure becomes stuck in the vicinity of conical intersection (CI) that precedes the elimination of the nitrogen. Prior to the elimination, the N_2 moiety assumes the direction quasi-perpendicular to the benzene ring.

This observation is in line with the deactivation of the S₂ state in **1** and **2** via locally non-planar conformations of the CI as was observed in the non-adiabatic MD runs.²²

Table 1. The strongest transitions in the transient spectra of **1**, **2**, and **3** for the relevant spectral region computed at the S₀ (FC) minimum geometries.

	$I \rightarrow F$ ^a	f ^b	E /nm
1	1 → 12	2.17×10^{-1}	360
	1 → 23	1.32×10^{-1}	304
	2 → 34	1.72×10^{-1}	474
	2 → 29	1.42×10^{-1}	516
	3 → 40	1.22×10^{-1}	458
2	1 → 15	2.69×10^{-1}	320
	2 → 20	1.99×10^{-1}	585
	2 → 25	1.94×10^{-1}	513
	3 → 29	9.88×10^{-2}	496
3	1 → 15	1.74×10^{-1}	324
	2 → 20	2.05×10^{-1}	590
	3 → 29	1.07×10^{-1}	504

^a Initial (I) and final (F) singlet excited states

^b Oscillator strengths in the length representation

In the S₁ state, the charge is transferred mainly locally within the C-N-N π-system. While this also weakens the C-N bond, the effect is less pronounced than in S₂. Consequently, it is possible

to optimize stable S_1 minima of **1**, **2**, and **3**. In these minima the C-N bond is on average elongated by 0.07 Å relative to the ground state and the N_2 moiety is tilted (the C-N-N angles are $\sim 130^\circ$; Fig. 2). However, unlike the situation in S_2 , the diazo group remains bonded to the C atom (although the bond length now approaches that of the single C-N bond), and its axis remains more aligned with the benzene ring plane; the corresponding angles equal 33° (**2**) and 19° (**3**). This also agrees with the findings from the non-adiabatic MD runs, which indicated that the radiationless decay of S_1 takes place predominantly via locally quasi-planar conformations of the S_1/S_0 CI.²²

The T_1 minima of **1**, **2**, and **3** show similar features as the S_1 minima; namely, the weakened but preserved C-N bond and the tilted N_2 moiety (Fig. 2). The T_1 states of **2** and **3** absorb in the 400-420 nm region (vide infra), which can be correlated to the TD-CAM-B3LYP computed lowest transitions at 402 (**2**) and 478 (**3**) nm. This wavelength difference is attributable to the notable difference in conformations of **2** and **3** in the T_1 state; in **2** the N_2 and benzene chromophores close the angle of ca. 70° while in **3** this angle is only ca. 30° . Although typically produced via inefficient intersystem crossings (ISC), the long-lived T_1 states are of interest as alternative precursors to the triplet carbenes which may in turn explain the observed ketone photoproducts.

Focusing on the spectra of the singlet and triplet **car-1-3** transients, the used TD-CAM-B3LYP and CASPT2 methods here exhibit some important differences (Figs. S18-S20 in the SI). For the singlet carbenes, TD-CAM-B3LYP predicts the strongest maxima as considerably blue-shifted and completely overlooks the significant features in the region of ca. 350-450 nm which is in discord with the experimental TA data (vide infra). The spectra of the triplet carbenes agree better for **car-2** and **car-3** but the discrepancies remain for **car-1**. Also, TD-CAM-B3LYP generally predicts much larger oscillator strengths than CASPT2. Considering the extensively

documented multiconfigurational nature of carbenes,⁴⁹ we consider the CASPT2 spectra to be more reliable even though there could be somewhat larger uncertainties in the oscillator strengths, which are presently computed as the dipole moment expectation values between the uncorrelated (CASSCF) wave functions.

Ultrafast transient absorption spectroscopy

fs-TA measurements for **1** in different solvents have been reported.^{38,43} We conducted fs-TA measurements for **1-3** in cyclohexane, upon excitation at 267 nm, which populates higher singlet excited states, S_2 and S_3 (the Franck-Condon states, FC) and we particularly focus on the early events after the excitation. The corresponding spectra are shown in Figs 4, 6 and 8. Global and target analysis of the transient data (using GloTarAn software⁵⁰), as well as single wavelength fitting was performed to extract characteristic time constants and to aid in data interpretation. To assign the bands in the fs-TA spectra of **1-3** we conducted computations of the ESA spectra for **1-3**, as well as the spectra of the corresponding singlet and triplet carbene intermediates. The comparison of our spectra for **1** and those in precedent literature^{38,43} with the computed ones, can serve as a benchmark to verify the validity of the level of theory used.

In the fs-TA spectra of **1**, at early times (<1 ps), a transient absorption spectrum was detected with clear maximum around 340 nm, and broad absorption stretching over almost whole visible region (Fig. 4A). Early transient spectrum decays within the temporal resolution of our setup with 238 fs time constant, revealing absorption of another species with maxima at 335 nm and around 360 nm. Two decay constants, 14.4 ps and 128.4 ps, describe dynamics for both of these two peaks. Longer time constant coincides with the rise of the long-lived positive feature at 325 nm detected at later delay times (Fig. 4B).

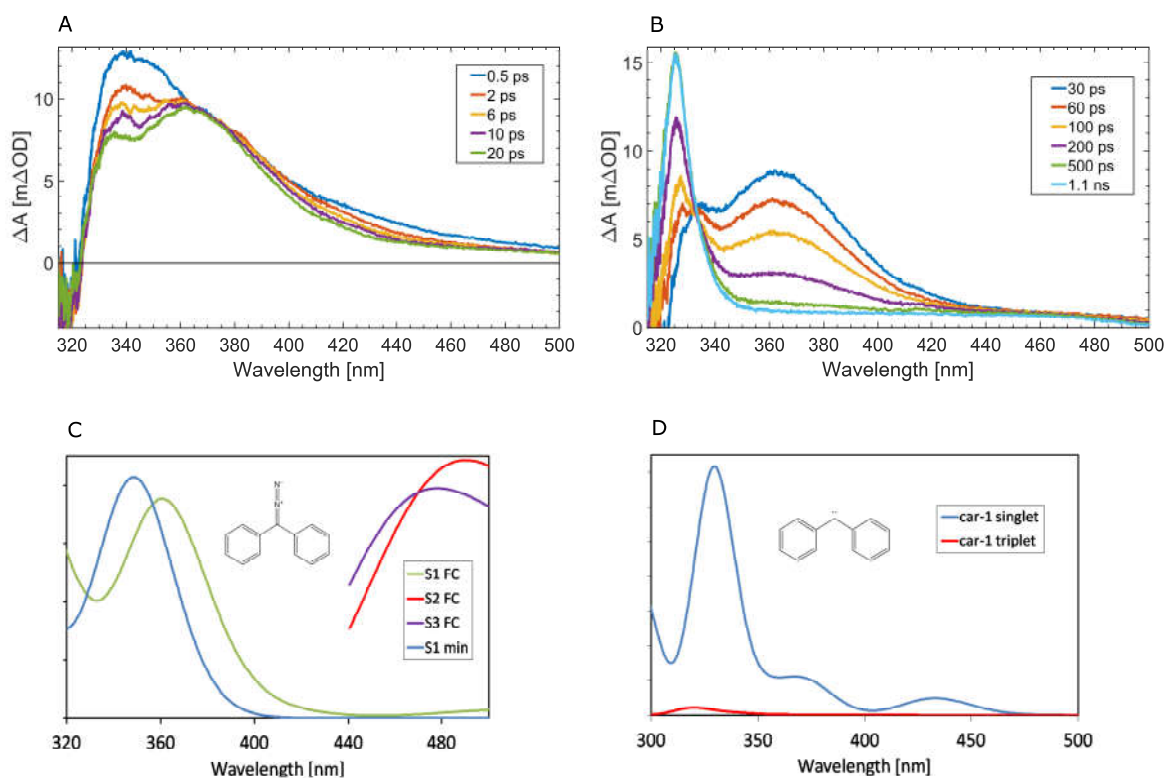


Figure 4. **A)** Transient absorption spectra of **1** upon excitation at 267 nm at early times. **B)** Later transient absorption spectra of **1** up to 1.1 ns probe delay. **C)** and **D)** The excited state absorption spectra computed for **1** and **car-1**. “S₁ FC” and “S₂ FC” are computed at the ground state (S₀) minimum while “S₁ min” is computed at the S₁ minimum. The spectra are convoluted with the Gaussian profiles (fwhm = 3000 cm⁻¹).

Model used for target analysis and its results for fs-TA spectra of **1** (Fig. 5) consists of 4 compartments (other tested models are shown in Fig S4 in the SI). Species associated spectrum of the first compartment (SAS1, Fig. 5A) was assigned to initially excited FC state of **1**, and it is in relatively good agreement with the calculated **1**(S₂) excited state absorption (ESA) above 450 nm shown in Fig. 4C. Here we note similar assignment of this broad spectrum to initially excited singlet state absorption in other fs-TA experiments.³⁹

Two new species are formed from the FC state in parallel processes. Shoulder at 360 nm, already observed after 1 ps, corresponds to the singlet carbene formed from **1**, **car-1** (compartment 3). The signal around 335 nm was assigned to the relaxed S₁ state of molecule **1** due to overlapping of SAS2 and calculated spectrum of the relaxed S₁ state. Most of the **car-1** population is formed from the initially excited FC state of **1**, but small part could be formed through inefficient photoelimination of nitrogen via a locally planar conical intersection (CI) from the relaxed S₁ state of **1** as was also suggested by computations.²² The formation of **car-1** from the relaxed S₁ was included in our model as it resulted in increased quality of the global fit.

Relaxed S₁ state further decays into ground state of **1** (14.4 ps). The singlet carbene decays with the time constant of 128.4 ps, forming new species absorbing at 325 nm, with a clear isosbestic point in the fs-TA spectra around 330 nm. The species absorbing at 325 nm was assigned to the triplet carbene from **1**, and the rate constant for its formation is in line with precedent literature for the intersystem crossing (ISC) in diphenylmethylen in nonpolar solvents.^{38,39} Decay of triplet **car-1** could not be resolved in our fs-TA measurements. By comparing measured and calculated spectra shown in Fig. 4 it can be seen that for singlet carbene there is substantial difference in spectral shape where only minor peak in the calculated spectra around 370 nm corresponds to our measurements. Here we note that calculated oscillator strengths are less reliable than corresponding spectral positions and it is possible that maximum around 430 nm, which we don't observe experimentally, is much weaker than the one at 370 nm, which coincides with the measured spectra assigned to singlet **car-1**. The maximum around 335 nm could be overlapped with ESA from **car-1** in triplet state and its amplitude could be much weaker than the calculated value as well. In addition, the calculated maxima for singlet state carbene generally

appear at longer wavelengths compared to the triplet, which is in good agreement with the experimental data.

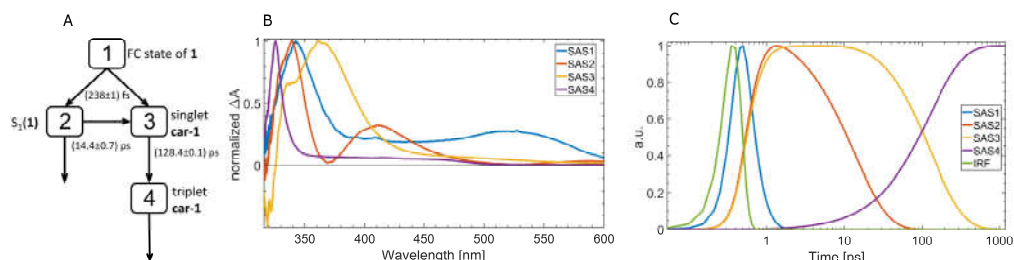


Figure 5. **A)** Model for target analysis of **1** that produced the best global fit results. **B)** Species associated spectra (SAS) corresponding to the four compartments of the target model of **1**. **C)** Normalized time profiles of the Species associated spectra and Instrument response function for the corresponding target analysis model, shown in logarithmic time scale.

In the fs-TA spectra of **2**, at early time after the 267 nm excitation, the transient absorption is detected with a maximum at 326 nm and shoulders stretching to 450 nm (Fig. 6A). We assume that this early absorption spectrum corresponds to initially excited S₂ FC state of **2**. As it is also the case for **1**, the computations of the ESA spectra from the S₂ and S₃ FC states of **2** predict intense features in the visible range (450 nm and above). We note that the modeled S₂ and S₃ spectra are cut off at the onset of the first ionization threshold, i.e. some 2.7-2.8 eV above S₂/S₃. Fast dynamics of the fs-TA spectra of **2** is described with biexponential decay. Extracted time constants are 910 fs and 25 ps. After initial fast decay, the measured spectrum consists of a negative signal at ≈300 nm due to irreversible ground state bleach of molecule **2** and positive signal with a maximum around 320 nm.

Model consisting of three compartments that was used in target analysis of the measured data is shown in Fig. 7. We assign the broad spectra of SAS1 to the initially populated FC state of **2**. It decays with the time constant of 940 fs and populates compartments 2 and 3 that correspond to **2**(S₁) and singlet carbene (**car-2**), respectively. SAS2 is in good agreement with the computed ESA of **2**(S₁ min) depicted in Fig. 6B. Model allows for additional (inefficient) formation of singlet carbene from **2**(S₁) state. Since the ground state bleach is irreversible and the decay of the third compartment is much longer than the available time delay window, they are both represented in SAS3. While it is expected that singlet carbene formation occurs in parallel processes from the FC state,²² there is significant discrepancy between the calculated spectra peaking at 390 nm and very broad SAS3 having maximum at much shorter wavelengths around 325 nm.

Alternative interpretation of the compartments matches SAS3 to the ESA of the triplet excited state **2**(T₁), whereas both **car-2** and **2**(S₁) would be represented by the second compartment with significant spectral overlap and similar temporal decay. It is anticipated that the triplet excited state can be populated via ISC from both FC state and **2**(S₁). However, since ISC is a spin forbidden process, it is expected to take place mainly from the relaxed S₁ state, as it should be slower compared to IC from the FC state to the relaxed S₁, which does not fit well with the model represented in Fig. 7. Moreover, it should be noted that LFP measurements detected **2**(T₁) absorbing at longer wavelengths around 420 nm (vide supra), rendering assignment of compartment 3 to **2**(T₁) less likely. Consequently, the best fit of the global model to experimental data corresponds to the assignment of compartment 2 to **2**(S₁), and compartment 3 to **car-2**. Furthermore, the largest part of **car-2** is formed directly from the FC state in the anti-Kasha photochemical reaction.

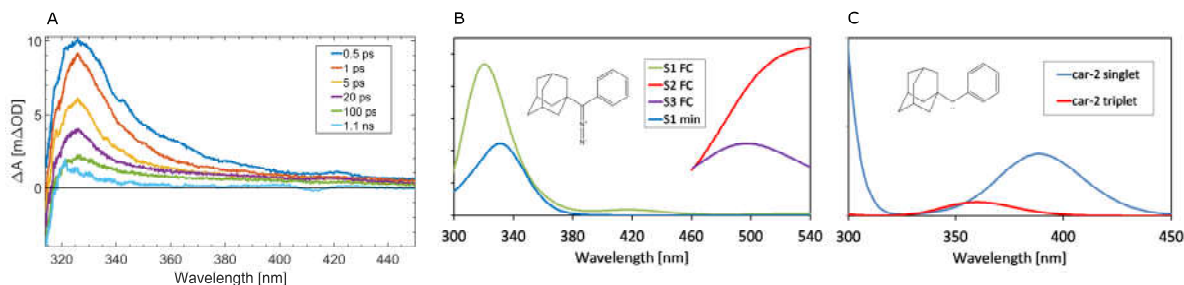


Figure 6. A) Transient absorption spectra of **2** upon excitation at 267 nm. B) and C) The excited state absorption spectra computed for **2** and **car-2**. “S₁ FC” and “S₂ FC” are computed at the ground state (S₀) minimum while “S₁ min” is computed at the S₁ minimum. The spectra are convoluted with the Gaussian profiles (fwhm = 3000 cm⁻¹).

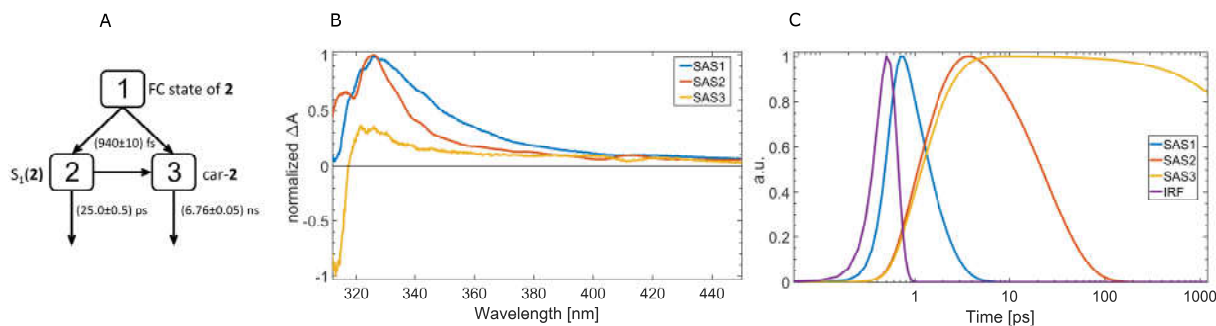


Figure 7. A) Model for target analysis of **2** that produced the best global fitting results. B) Species associated spectra (SAS) corresponding to the three compartments of the target model of **2**. C) Time profiles of the Species associated spectra and Instrument response function for the corresponding target analysis model, shown in logarithmic time scale.

The fs-TA spectra of **3** (Fig. 8A) are similar to those from **2**. Both samples exhibit biexponential fast decay of the positive absorption bands, and long-lived negative ground state bleach signal. However, there is important distinction. By comparing TA spectra at longest delay point, it can be seen that in **2** there is still some positive signal above 320 nm that is not present in **3**. We used three compartments to describe the data using global target analysis (Fig. 9). Spectra belonging to first two compartments correspond to the initially excited FC state and the relaxed singlet excited **3**(S₁) state. Dynamics of these states is described by 2.2 ps decay for the FC state and

19.2 ps decay for the S_1 . Spectral position of the $\mathbf{3}(S_1)$ agrees with the calculated ESA of $\mathbf{3}(S_1)$ from Figure 8B. The third compartment in target analysis was introduced to describe long-lived ground state bleach that indicates additional pathway of the photoreaction from the initially excited state. Based on identification of photoproducts (*vide infra*), we suspect that it corresponds to the irreversible formation of stable alkene **15** that does not absorb at 300 nm. Results of global analysis using another (parallel) model that produced reasonably good fitting results are shown in Fig S5 in the SI. The negative signal observed in the fs-TA spectra could in principle correspond also to the stimulated emission from higher excited state of **3**. However, the detected fluorescence spectrum of **3** stretches to 420 nm (Fig S2 in the SI), whereas the negative signal in the fs-TA was observed at $\lambda < 350$ nm, indicating that it is due to the ground state bleach. The stimulated emission was probably not detected due to its low intensity and overlapping with the positive transient absorption.

Note that the negative signal is (according to the global fit) formed at early times after the excitation, within resolution of the setup. This indicates that the formation of **car-3** and subsequent H-insertion to **15** take place ultrafast from the initial FC state in another anti-Kasha photochemical reaction. The other option is that **car-3** is never formed and that **15** is produced directly in the RIES process from the FC state of **3**. Most probably **car-3** has a low absorptivity, as it is the case of **car-2** whose absorption band was covered by the absorption of $\mathbf{2}(S_1)$. Moreover, anticipated short lifetime of the singlet **car-3**, due to formation of **15**, makes it difficult to be detected by transient spectroscopy. Thus, detection of **car-3** remains elusive.

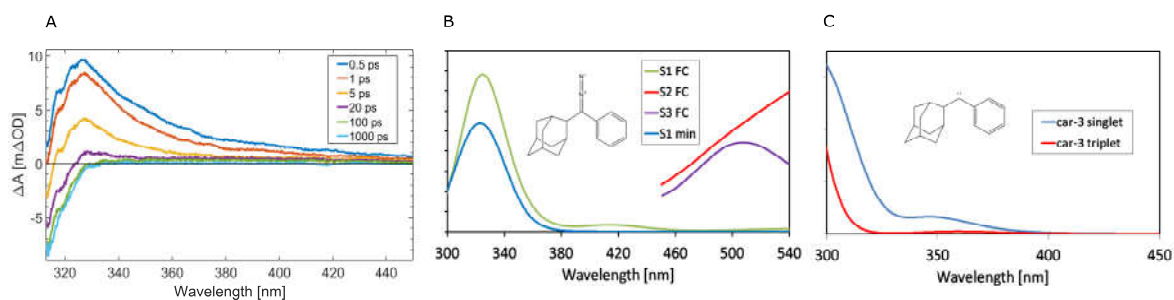


Figure 8. A) Transient absorption spectra of **3** upon excitation at 267 nm. B) and C) The excited state absorption spectra computed for **3** and **car-3**. “S₁ FC” and “S₂ FC” are computed at the ground state (S₀) minimum while “S₁ min” is computed at the S₁ minimum. The spectra are convoluted with the Gaussian profiles (fwhm = 3000 cm⁻¹).

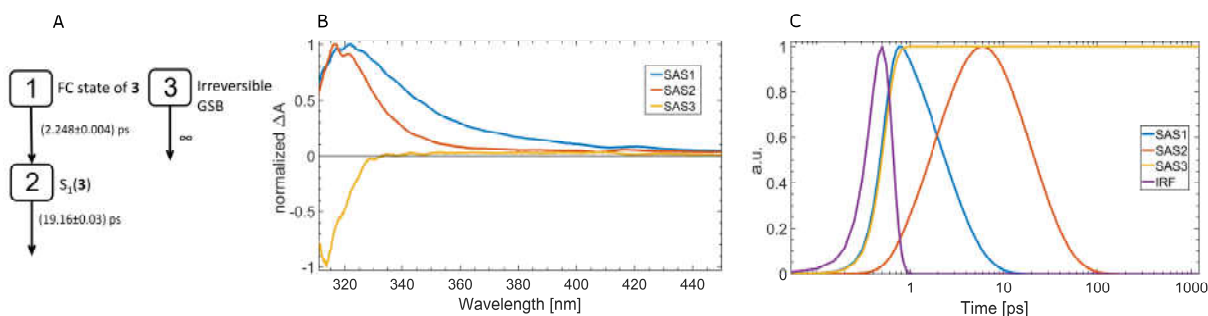


Figure 9. A) Model for target analysis of **3** that produced the best global fitting results. B) Species associated spectra (SAS) corresponding to the four compartments of the target model of **3**. C) Time profiles of the Species associated spectra and Instrument response function for the corresponding target analysis model, shown in logarithmic time scale.

Laser Flash Photolysis

Photochemistry of **1** has been intensively investigated by both laser flash photolysis (LFP) and fs-TA.³¹⁻⁴² To detect plausible longer-lived reactive intermediates in the photochemistry of **2** and **3**, we conducted LFP measurements. The experiments were performed upon excitation with a YAG laser at 266 nm in pentane solution at rt or at -90 °C. The solution was purged with N₂- and O₂ where we expected that O₂ would quench triplet excited states and triplet carbenes (for all

LFP data see figs S6-S14 in the SI). Photochemical reaction on a similar molecule **Nor-1** (Fig. 10) has been investigated by Tomioka et al.⁵¹ whereas Platz et al.,⁵² studied the corresponding diazirine-1. Tomioka et al. detected a transient in degassed benzene absorbing at 430 nm that decayed giving a new transient absorbing at 320 nm. The decay of the first transient with the lifetime of $\tau = 5.6$ ms was correlated with the rise of the second transient absorbing at 320 nm, decaying over much longer time-scale. They assigned the primary transient at 430 nm to 1-phenyladamantene, whereas the transient at 320 nm was assigned to a dimerization product of 1-phenyladamantene (Fig. 10). On the other hand, Platz et al. observed only one transient absorbing at 320 nm, assigned to adamantene that decayed over millisecond time-scale, but not with unimolecular kinetics.⁵² For both anti-Bredt olefins the rate constants with different quenchers were reported including O₂ (10^6 - 10^7 M⁻¹s⁻¹) and CH₃OH (10^2 - 10^4 M⁻¹s⁻¹).^{51,52}

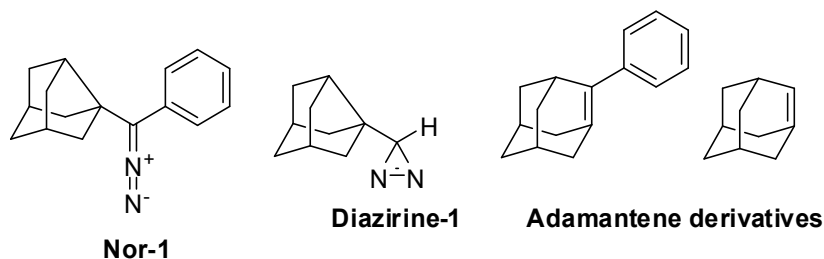


Figure 10. Diazo- and diazirine molecules and the corresponding intermediates investigated by Tomioka and Platz.^{51,52}

In the N₂- and O₂-purged pentane solution of **2** (Fig S6 in the SI) two transients were detected, similar to the results of Tomioka et al. However, the transients decayed over much shorter time-scale (Fig S7 in the SI). The first transient was formed within the laser pulse. It had a lifetime of 750 ± 100 ns ($k = 1.3 \times 10^6$ s⁻¹) and absorbed in the region 300-600 nm with a maximum at ≈ 400 -420 nm. Its decay took place during the rise of the second transient absorbing at shorter wavelengths with a maximum at ≈ 350 nm. The rise of the second transient was faster (k

$=3.3 \pm 0.2 \times 10^6 \text{ s}^{-1}$) than the decay of the first. The second transient had longer lifetime of 10-15 μs (Fig. 11). After the decay of both transients, residual absorption was detected, probably corresponding to the formation of stable azine product absorbing over the whole spectrum.

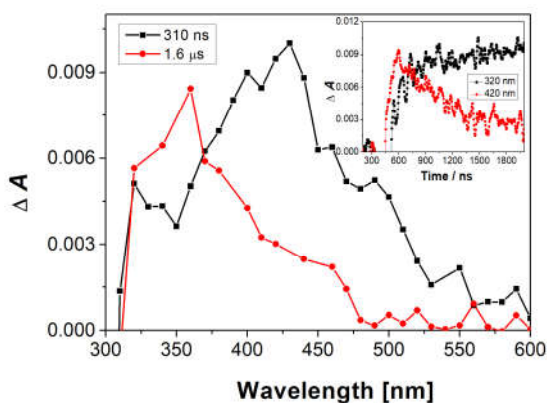


Figure 11. Transient absorption spectra of **2** ($c = 1.83 \times 10^{-4} \text{ M}$) in N_2 -purged pentane solution (at rt) with a delay of 310 ns, or 1.6 μs after the laser pulse (266 nm). Inset: Growth kinetics at 320 nm and decay kinetics at 420 nm.

In the O_2 -purged pentane solution of **2**, the first transient (420 nm) was quenched and had the lifetime of $45 \pm 10 \text{ ns}$ (for the spectra in the presence of quenchers see Figs S8 and S9 in the SI). Taking the value of O_2 solubility in pentane at $20 \text{ }^\circ\text{C}$ of $17.7 \times 10^{-3} \text{ M}^{53}$ the shortening of the lifetime corresponds to k_q of $1.2 \times 10^9 \text{ M}^{-1}\text{s}^{-1}$. This rate constant is similar to the values for the quenching of triplet excited states and triplet carbenes by O_2 , whereas singlet carbenes react with O_2 slower with the rate of $k \approx 10^7 \text{ M}^{-1}\text{s}^{-1}$.⁵ Note that the characteristic signal of carbon monoxide usually observed by the quenching of carbenes by O_2 ³³ was not detected. The second transient (320 nm) was not quenched with O_2 . LFP experiment in the presence of pyridine, a ubiquitous carbene quencher, could not be performed due to the absorption of pyridine at 266 nm. Methanol is a good quencher of singlet carbenes ($k_q = 10^8 - 10^9 \text{ M}^{-1}\text{s}^{-1}$) and triplet carbenes

($k_q = 10^5 - 10^7 \text{ M}^{-1}\text{s}^{-1}$).^{4,5} However, CH₃OH did not quench the first transient (420 nm). In the N₂-purged solution in the presence of 0.1 M CH₃OH the lifetime of the first transient was even slightly longer $850 \pm 100 \text{ ns}$. On the contrary, in the presence of CH₃OH the second transient (320 nm) was not detected, suggesting that its formation involved carbene intermediates, and presumably, did not involve the first transient (420 nm). Based on the above discussion, the first transient (420 nm) was tentatively assigned to the triplet excited state of **2**. This triplet excited state is most probably not involved in the formation of products reported in literature precedent,²² except ketone. Based on the work of Tomioka⁵¹ and Platz⁵², the second transient (320 nm) is tentatively assigned to anti-Bredt olefin, product **16** (Scheme 3).

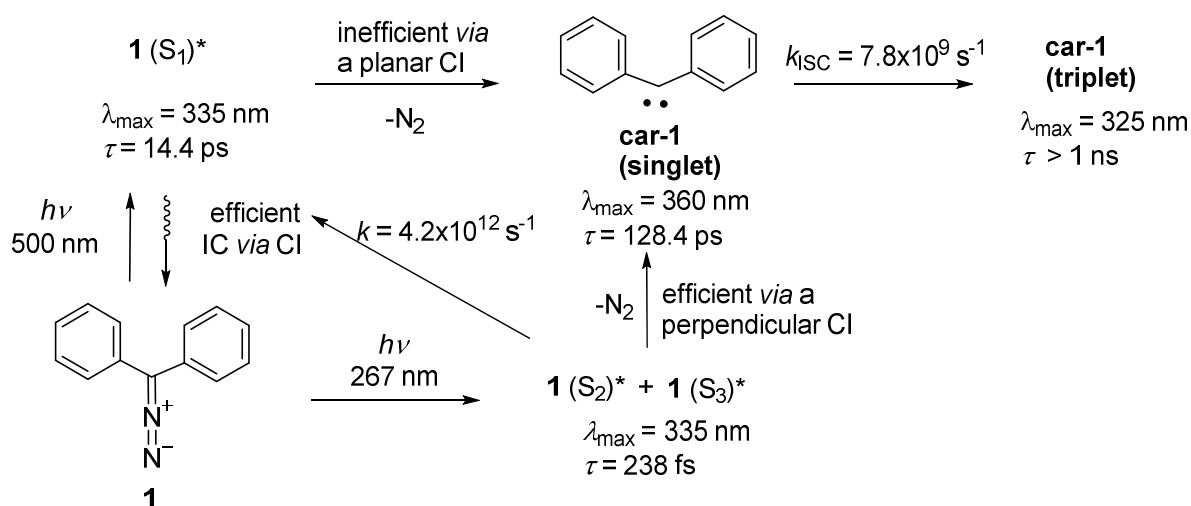
In the N₂-purged pentane solution of **2** at -90 °C two transients were detected (Figs S13 and S14 in the SI). The first is short-lived, $\tau = 300 \pm 100 \text{ ns}$, and absorbs in the region 320-400 nm. The other transient is longer-lived and absorbs almost over the whole spectrum with a maximum at 400-420 nm. The lifetime of the second transient is $5.2 \pm 0.2 \text{ }\mu\text{s}$. Its formation could be time-resolved; it was formed with the rate constant of $k = 7 \pm 2 \times 10^6 \text{ s}^{-1}$. Contrary to the pentane solution at rt, very long-lived transient that was assigned to olefin **16** was not detected (maximum at 350 nm, $\tau = 10\text{-}15 \text{ }\mu\text{s}$). In O₂-purged solution, only a very weak transient was detected at 400-420 nm with the lifetime of $\approx 30 \text{ ns}$. From the lifetimes in N₂- and O₂-purged solution rate constant for the quenching of long-lived transient at 400-420 nm is $k_q \approx 2 \times 10^9 \text{ M}^{-1}\text{s}^{-1}$. Based on the study at -90 °C, quenching with O₂ and computations, the transient with the lifetime of 300 ns detected at -90 °C only was tentatively assigned to the triplet state of car-**2**, whereas the transient with the lifetime of 5 μs probably corresponds to the triplet excited state of **2**.

In the N₂- and O₂-purged pentane solution of **3** (Fig S11 and S12 in the SI), a transient was observed absorbing at 300-550 nm with a maximum at 400-420 nm. Its formation could not be time-resolved; it took place during the laser pulse. The decay of the transient in N₂-purged solution followed unimolecular kinetics with the lifetime of 1.0 ± 0.1 μs. The decay of the transient was faster in O₂ purged solution with the lifetime of 120 ± 10 ns, which roughly corresponds to k_q of $\approx 4.1 \times 10^8$. Based on the findings for **2**, the transient was tentatively assigned to the triplet excited state of **3**. After the decay of the triplet no additional longer-lived transient was observed. However, absorption spectra after LFP (Fig. S10) indicate formation of stable product with an absorption band at shorter wavelengths, ca. 250 nm. This absorption corresponds to photoproduct **15** formed by the C-H insertion, which was isolated and fully characterized. **Car-3** was not detected. However, isolation of ketone **13** strongly indicated that it was formed via triplet carbene **car-3**.

Reaction mechanisms

Based on previous discussion, in Scheme 2 we present reaction pathways of **1**. UV pulses at 267 nm excite initial molecule to the S₂ and S₃ FC states. From there, the nitrogen elimination reaction takes place efficiently producing **car-1** in the singlet state via locally perpendicular CI.²² This confirms that formation of **car-1** falls under anti-Kasha photochemistry. Initially excited FC state of **1** also goes through IC to **1**(S₁) state, which further relaxes to the ground state of **1** through efficient IC via conical intersection. **car-1** can also be formed inefficiently from **1**(S₁) via a locally planar CI.²² Singlet carbene undergoes ISC with 128.4 ps time constant to the

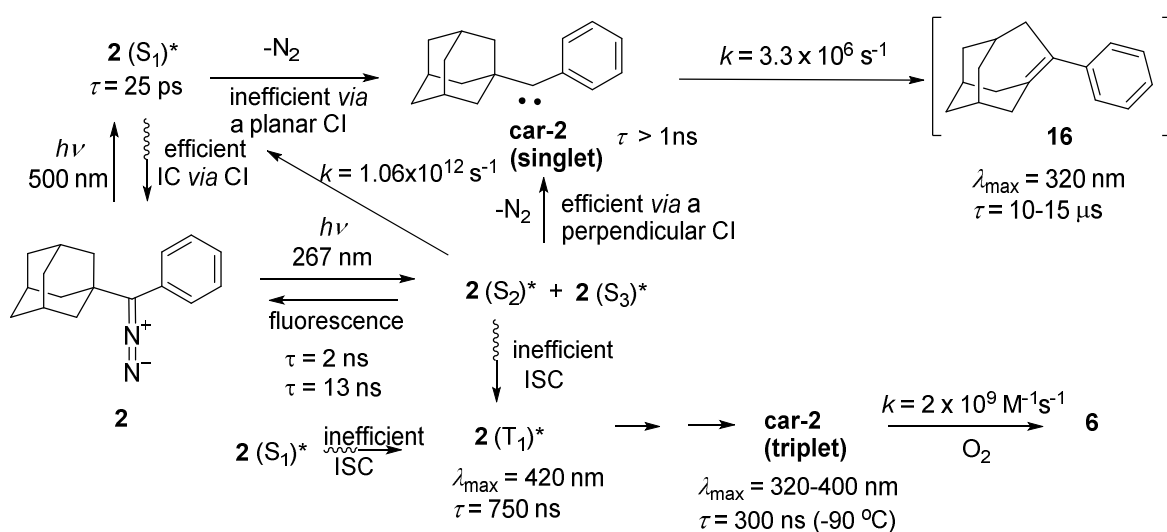
ground triplet state, which is more stable by 5.3 kcal mol⁻¹ according to the CASPT2 method (vide supra). Both carbene species can be intercepted with different reagents/molecules, which was studied in detail in literature precedent.³²⁻⁴³



Scheme 2. Photochemical pathways of **1**.

The light excitation of **2** at 267 nm populates the S₂ and S₃ FC states, which relax to the S₁ with the time constant of 940 fs. Concomitantly, in the competing photochemical reaction taking place from the FC state, elimination of nitrogen via CI takes place, delivering **car-2** in the singlet state (Scheme 3). The time-resolution for the N₂ elimination could not be resolved from the IC process delivering **2**(S₁), but there is an undeniable evidence that **car-2** is mainly formed directly from the FC state of **2** in the ultrafast reaction. Thus, elimination of N₂ is much more facilitated from the S₂ or S₃ state than from S₁. In case of **2**, fs-TA spectra did not reveal ISC process from the singlet **car-2** to the triplet. The singlet carbene deactivates by insertion into the C-C bond of adamantane giving anti-Bredt olefin **16**, tentatively detected by LFP, and it reacts with solvent in a bimolecular reaction delivering C-H insertion products, which were documented previously.²²

Thus, singlet carbene **car-2** has longer lifetime, most probably in the range of 1-10 ns, which cannot be measured by our fs-TA or ns LFP setups. Note that the energy difference between the singlet and triplet carbenes is the largest among the investigated. Thus, ISC process in this case is the slowest and in competition with the unimolecular C-C insertion reaction, or bimolecular C-H insertion with the solvent.



Scheme 3. Photochemical pathways of **2**.

Table S6 shows the computed rate constants and reaction free energies for the insertion of the singlet **car-2** into the adjacent C-C bond. Fig. S21 depicts the corresponding transition state and product **16** optimized at the CAM-B3LYP(+PCM)/6-311+G(2d,p) level. The rate constant for this reaction computed using the hybrid meta-GGA density functional M06 ($k = 1.2 \times 10^6 \text{ s}^{-1}$) is in the best agreement with the measured value of $3.3 \times 10^6 \text{ s}^{-1}$ (Scheme 3). This is in line with our previous findings, viz. in the DFT/PCM setting hybrid GGA functionals (e.g. M06, PBE0 and B3LYP) perform better for the activation barriers and rate constants than range-separated

hybrids.⁵⁴ The reaction free energies are in good agreement for all the tested functionals with the estimated value of (-36 ± 2) kcal mol⁻¹.

The singlet excited state of **2** (the FC state or relaxed S₁) also undergoes inefficient ISC, populating the triplet excited state of **2**, which was detected by LFP. Most probably, formation of the triplet carbene **car-2**, detected by LFP at -90 °C can be rationalized as species formed from **2**(T₁). Formation of adamantyl phenyl ketone photoproduct is also a strong indication for the involvement of triplet carbene **car-2** in the photochemistry of **2**.²² Thus, LFP and fs-TA allowed for the detection of both singlet and triplet carbene **car-2**, whereas fs-TA showed also evidences that N₂ elimination from **2** takes place from the FC state in the anti-Kasha photochemical reaction.

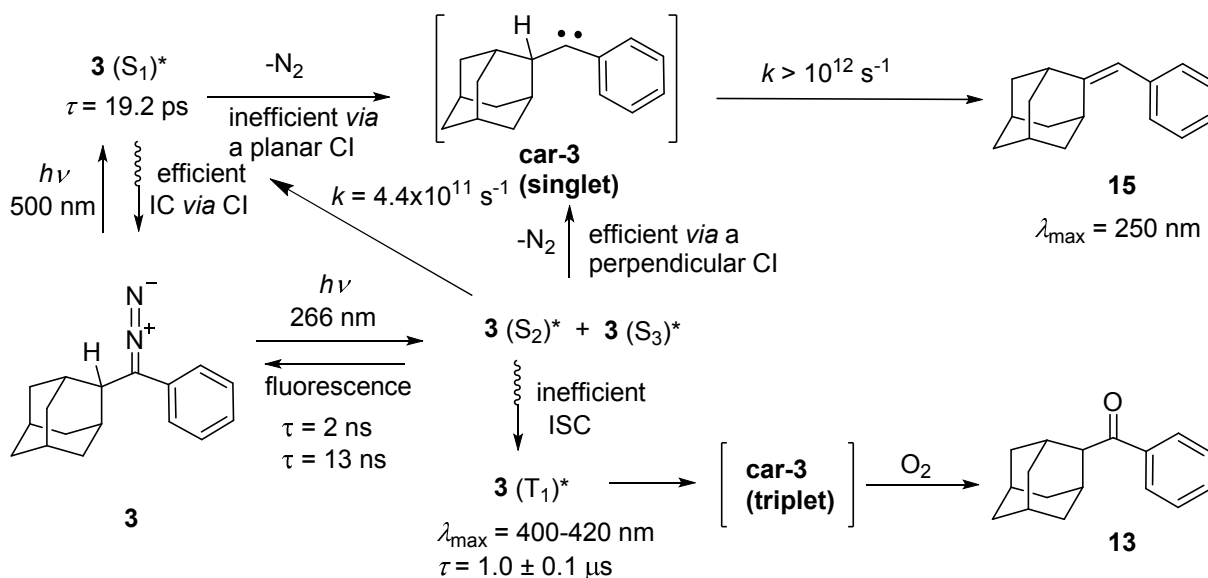
Due to the same type of chromophore in **2** and **3**, one would expect similar photophysical properties and photochemical pathways in early times after the 267 nm excitation. The early FC spectra computed for **2** and **3** (Figs 6 and 8) show only minor differences. These are mainly due to the differences in the minimum conformations, specifically the mutual positions of the phenyl and N₂ chromophores. Similar to the observed pathways for **2**, after the population of the FC state upon the light absorption at 267 nm, the system deactivates by IC to the relaxed **3**(S₁) and by N₂ elimination to deliver **car-3** that is expected to react via the insertion into the α C-H bond furnishing stable photoproduct, alkene **15** (Scheme 4). The reaction, which can also be thought of as a hydrogen atom transfer from the α-C to the carbene C, is characterized by an early transition state (Fig. S21 in the SI), hence is exceedingly fast and exothermic with the CAM-B3LYP rate constant of $>10^{12}$ s⁻¹ ($\Delta G^\ddagger = 1.3$ kcal mol⁻¹) and the reaction free energy of -67 kcal mol⁻¹. Thus, although the singlet **car-3** exists as a minimum on the free energy surface, it is very

shallow and fleeting with the upper lifetime bound at 298 K in the subpicosecond time scale. Indeed, the facile torsion around the $>\text{C}(\text{H})\text{-C}_{\text{carbene}}$ bond approximates the reaction coordinate well; the relaxed scan with respect to this mode is sufficient to trigger the rearrangement of the singlet **car-3** to the photoproduct **15**. This, in addition to its low absorptivity, precludes its detection by the fs-TA.

On the other hand, photoproduct **15** might form directly from the FC state of **3** in the RIES process, thus circumventing the carbene species. Since the negative bleach signal due to the irreversible formation of **15** is detected at very early times after the excitation in parallel to the relaxation to **3**(S_1), our experiments strongly indicate that it is another example of the anti-Kasha photochemical reaction. The relatively large energy gap between S_2 and S_1 (see the SI) allows for the competing IC and photochemical pathway delivering **car-3** or **15**. Furthermore, note that we have also detected fluorescence from the upper singlet excited states of **3**, which further supports this anti-Kasha reactivity.

While we have no spectroscopic evidence for the formation of the singlet **car-3**, the isolation of ketone **6** in the photochemistry of **3** is a strong indication that triplet **car-3** was present in the photochemical reaction. According to the CASPT2 method, the triplet **car-3** is by $7.3 \text{ kcal mol}^{-1}$ more stable than the corresponding singlet. It is most probably formed from the triplet excited state of **3**, which was detected by LFP. The triplet excited state of **3** can be formed from the FC state of **3**, or from the relaxed S_1 state. Although we did not detect the triplet carbene **car-3**, it should have longer lifetimes compared to the singlet since it should not undergo synchronous α C-H insertion. The lack of the triplet **car-3** detection is probably due to its inefficient formation.

Overall, after excitation of **3** at 267 nm, the main pathway involves anti-Kasha singlet reactivity delivering stable photoproduct **15**.



Scheme 4. Photochemical pathways of **3**.

As discussed above, the singlet-triplet ISC of **car-1-3** can compete with their reactions with the solvent and intramolecular rearrangements. However, our attempts at computing the corresponding ISC rates using the path integral formalism⁵⁵ failed. This is presently caused by the observed breakdown of the harmonic FCHT approximation (indicated by the too large values of the norm of the displacement vector in the Duschinsky transformation). We still note that, owing to the significantly smaller S-T gap in **car-3**, the ISC rate from **car-3** should be significantly faster than that from **car-2** subject to both compounds having comparable spin-orbit couplings. Still, owing to the ultrafast α -C-H insertion in **car-3** the ISC yields should be negligible compared to the formation of the alkene **15**.

Finally, the computations provided some hints as to the conceptually and practically important reactivity of the studied diazo compounds and their photochemical transients in excited states, especially with regards to the possibility of the RIES. The S_2 state is again confirmed as an efficient precursor to the elimination of N_2 since the attempts at optimizing the S_2 minima of **1**, **2**, and **3** with the C-N bond preserved were unsuccessful. To estimate the feasibility of the N_2 elimination from the S_1 and T_1 states, beginning with the S_1 and T_1 minima we performed relaxed surface scans by gradually extending the C-N bond. At the TD-CAM-B3LYP level, the C-N bond dissociation energies are similar for **2** and **3**, approximately 14 kcal mol^{-1} from S_1 (at which point the CI with the ground state is encountered), and $12\text{-}13 \text{ kcal mol}^{-1}$ from T_1 .

The conformational features of the structures from the relaxed scans do not furnish evidence that the N_2 elimination in the excited states might be concerted with the insertion into the α C-H bond. Namely, the process of the C-N bond dissociation in S_1 and T_1 is not accompanied by the torsion around the $>C(H)-C_{\text{carbene}}$ bond that would enable the concomitant α C-H insertion (vide supra). The similar observation applies to the conformations in the vicinity of the CI that gives rise to the N_2 elimination. We note, however, that the relaxed scans may diverge from the true reaction paths, and so more reliable answers as to the possibility of the RIES could be obtained from non-adiabatic dynamics, although this has thus far been unfeasible owing to the large size of the adamantyl derivative.²²

Conclusions

Photochemical reactivity of diazo compounds **1-3** and the corresponding carbenes was investigated computationally using the methods of time-dependent density functional theory (TD-CAM-B3LYP) and multiconfigurational perturbation theory to the second order as well as

experimentally by transient spectroscopy. We provide the first spectroscopic evidence that the elimination of N₂ from diazo compounds upon excitation at 267 nm takes place in the anti-Kasha ultrafast photochemical reaction, within 1 ps, directly from the upper excited singlet states. The singlet carbenes from **1** ($\lambda_{\text{max}} \approx 360$ nm, $\tau = 128.4$ ps) and **2** ($\lambda_{\text{max}} \approx 325$ nm, $\tau > 1$ ns) were detected by fs-TA. In addition, we detected triplet carbenes, formed by ISC from **car-1** ($\lambda_{\text{max}} = 325$ nm, $\tau > 1$ ns) or by the elimination of N₂ from the triplet excited state of **2** ($\lambda_{\text{max}} = 325$ nm, $\tau > 1$ ns). The reactivity of singlet carbenes differs with respect to the substituent at the carbene center. In nonpolar solvent they undergo ISC or insertion reactions into C-H and C-C bonds ($\lambda = 320$ - 400 nm, $\tau = 300 \pm 100$ ns at -90 °C). In particular, elusive singlet **car-3** should have a very short lifetime (upper limit of $\tau = 1$ ps) due to the presence of α C-H bond next to the carbene center and intramolecular C-H insertion reaction. This spectroscopic evidence that sheds light on the mechanism of carbene formation is important as it indicates that excitation to higher singlet excited states drives the efficient process, contrary to the well-accepted paradigms in organic photochemistry. Moreover, spectroscopic detection of different carbenes and rate constants for their reactions are important in planning reactivity and using such species in different processes, particularly in biology where the desired biological action can be in competition with numerous competing carbene pathways.

Experimental and Computational Details

General details, synthetic procedures for the preparation of all known compounds and description of photochemical and photophysical experiments is provided in the SI.

Synthesis of 2-Adamantyl Phenyl Ketone Hydrazone (14)

A solution of 2-adamantyl phenyl ketone (**13**) (1 mmol) and hydrazine monohydrate (20 mmol) in anhydrous MeOH (~ 10 mL) was refluxed for 24 h using an oil bath. The solvent was removed under reduced pressure and the resulting solid purified by column chromatography on silica gel (0-50 % diethyl ether in hexane) to yield the corresponding hydrazone in the form of colorless solid.

Colorless solid; isolated yield 30%; mp 138-140 °C (sublimes at 124-128 °C); ¹H NMR (300 MHz, CDCl₃): 7.40-7.47 (m, 2H), 7.31-7.38 (m, 1H), 7.17-7.23 (m, 2H), 5.01 (br.s, 2H), 2.73 (br.s, 1H), 2.07-2.18 (m, 2H), 2.03 (br.s, 2H), 1.79-1.93 (m, 4H), 1.69-1.78 (m, 4H), 1.46-1.56 (m, 2H); ¹³C{¹H} NMR (75 MHz, CDCl₃): δ 154.4, 134.5, 128.9, 128.1, 127.2, 50.6, 38.8, 37.7, 32.3, 29.5, 28.1, 27.9; IR (KBr) $\tilde{\nu}$ 3346 (m), 2904 (s), 2843 (m), 1442 (w), 740 (m), 689 (m) cm⁻¹; HRMS (ESI-TOF) m/z: [M+H]⁺ Calcd. for C₁₇H₂₂N₂ 255.1861; Found 255.1855.

Synthesis of diazo compounds **3**

To a suspension of a barium manganate (BaMnO₄, 8 mmol) and powdered CaO (55 mmol) in dry diethyl ether (~ 5 mL) was added a solution of hydrazone **14** (1 mmol) in dry diethyl ether (~ 5 mL) under a nitrogen atmosphere. The reaction mixture was stirred at rt for 1 h. Filtration of solids and evaporation of the solvent under reduced pressure afforded the corresponding diazo compound.

(2-Adamantyl)diazophenylmethane (3) pink colored waxy solid; isolated yield 98%; ¹H NMR (CDCl₃, 600 MHz): δ 7.32 (t, 2H, *J* = 7.9 Hz), 7.03 (t, 1H, *J* = 7.3 Hz), 6.97 (d, 2H, *J* = 7.9 Hz), 3.07 (s, 1H), 2.06 (br.s, 2H), 1.97-2.01 (m, 1H), 1.91-1.96 (m, 4H), 1.82-1.90 (m, 3H), 1.78 (br.s, 2H), 1.61 (d, 2H, *J* = 12.5 Hz); ¹³C{¹H} NMR (CDCl₃, 150 MHz): δ 131.7 (s, 1C), 128.8 (d, 2C), 123.4 (d, 1C), 122.6 (d, 2C), 38.5 (t, 2C), 38.4 (d, 1C), 37.4 (t, 1C), 32.6 (t, 2C), 29.8 (d, 2C), 27.8 (d, 1C), 27.1 (d, 1C), 1C not seen (C=N); IR (KBr) $\tilde{\nu}$ 2899 (s), 2847 (s), 2034 (s), 1596 (m), 1492 (m), 742 (m) cm⁻¹; UV: cyclohexane λ_{\max}/nm (log ϵ): 298 and 511 nm (4.21 and 1.55 M⁻¹ cm⁻¹), benzene: λ_{\max}/nm (log ϵ): 292 and 514 nm (4.23 and 1.68 M⁻¹ cm⁻¹); HRMS (ESI-TOF) m/z: [M+H]⁺ Calcd for C₁₇H₂₁N₂ 253.1705; Found 253.1716.

Femtosecond Transient Absorption

We investigated ultrafast dynamics of diazo derivatives on a homebuilt fs-TA experimental setup, which is detailed elsewhere.⁵⁶ Briefly, 120 fs pulses at 800 nm center wavelength at 1 kHz repetition rate were generated using Ti:sapphire regenerative amplifier system (Spitfire, Spectra-Physics). For the pump pulses, fundamental beam was frequency doubled to give 400 nm and then mixed with leftover fundamental beam to produce 267 nm via sum frequency generation. Pump pulses were chopped at 500 Hz frequency using synchronized mechanical chopper. Probe pulses were generated using small amount of fundamental beam that passes through delay line, which allows measurement up to ~ 1 ns. After the delay line, beam was focused in a 3 mm thick CaF₂ crystal, producing useful white light continuum spanning from 310 nm to 680 nm. Fundamental beam was eliminated from the probe beam using high reflectivity mirror. Magic angle between pump and probe polarizations was achieved by rotating probe polarization using a waveplate. Both beams were focused onto 0.5 mm path length quartz flow cell that has two 0.2 mm thick aperture windows (48/UTWA2; Starna) which was used to minimize coherent artifacts in transient absorption spectroscopy. After passing through the flow cell, probe beam is collimated and send to homemade spectrometer equipped with the detector (Hamamatsu S7030-1006) and a read-out electronics capable of single-shot measurement of the probe spectrum at the full 1-kHz laser repetition rate (Entwicklungsbuero EB Stresing, Berlin, Germany). We determined temporal resolution of 250 fs by fitting Gaussian function and its time derivatives on coherent artifact signals obtained in measurements in pure solvent. In order to keep reasonable signal to noise ratio, slightly higher pump fluences were used for adamantyl precursors **2** and **3**. Pump fluence was 1.13 mJ/cm², 4.19 mJ/cm² and 2.83 mJ/cm², for measurements on **1**, **2** and **3**, respectively.

Laser Flash Photolysis

All LFP measurements were performed on the University of Victoria setup, previously described.⁵⁷ The samples were excited with a pulsed Nd:YAG laser at 266 nm (<50 mJ per pulse), with a pulse width of 10 ns. Static cells (7 mm × 7 mm or 10 × 10 mm) were used, and they were frequently exchanged to assure no contamination with photoproducts. The solutions were purged with N₂ or O₂ for 20 min prior to performing the measurements. A Unisoku USP-203 cryostat placed at the position of the sample holder was used for the low temperature experiments.⁵⁸ Absorbances at 266 nm were 0.3-0.4. Details on the sample preparation for the LFP measurements can be found in the supporting information.

Computational Methods

The photochemistry of the studied compounds was modeled in the framework of density functional theory (DFT) and its time-dependent formalism (TD-DFT) using mainly the long-range corrected CAM-B3LYP hybrid density functional.⁵⁹ This functional has repeatedly been shown to reliably correct for the deficiencies of the parent B3LYP in case of the charge transfer and Rydberg excited states.^{59,60} The S₀ and T₁ minima of the three diazo- compounds (**1**, **2**, and **3**) and the corresponding singlet and triplet carbenes (**car-1**, **car-2**, and **car-3**) were optimized using the 6-311+G(2d,p) basis set. The lowest singlet excited state (S₁) minima of **1**, **2**, and **3** were optimized using the similarly sized minimally augmented Karlsruhe basis set ma-def2-TZVP(-f)^{61,62} exploiting the resolution of identity (RI) approach and auxiliary basis sets to accelerate the computations. Here, the non-local HF exchange term was evaluated using the chain-of-spheres (COSX) approximation which increases efficiency for hybrid density functionals.⁶³ The Coulomb term was fitted using the auxiliary def2/J basis set⁶⁴ and the split-RI-

J scheme,⁶⁵ the COSX and RI-J schemes combined give rise to the RIJCOSX approximation. In all the optimizations, the presence of the cyclohexane solvent was described in terms of the (conductor-like) polarizable continuum model (PCM),^{66,67,68} see the SI for details on the DFT integration grids, used algorithms and PCM molecular cavities. The equilibrium solvation was assumed in the optimizations and the non-equilibrium one in computing the vertical absorption spectra (vide infra). The Grimme's G3 atom-pairwise dispersion correction based on the Becke-Johnson damping function (G3BJ) was used throughout.⁶⁹

By optimizing the S_0 and S_1 minima of **1**, **2**, **3** with the CAM-B3LYP(+PCM) method, we obtained a set of reasonable geometries at which we computed the ESA spectra as an aid in the assignment of the relevant photochemical transients. The transition dipole moments between pairs of excited states were computed at the TD-CAM-B3LYP(+PCM)/ma-def2-TZVP(-f) level, and are approximated as the expectation values of the dipole moment operator between the Kohn-Sham configuration interaction singles (CIS) (pseudo)wavefunctions resulting from the Tamm-Dancoff approximation.⁷⁰ At the ground state ("Franck-Condon", FC) geometries as the initial states we considered S_1 , S_2 , and S_3 whereas at the S_1 minima only the S_1 state. The ESA spectra were built on the basis of up to 45 calculated TD-DFT roots, which were sufficient to cover the spectral range of interest (300-700 nm, and up to the first ionization threshold in case of S_2 and S_3). For the pairs of the excited states involved in the most intense ESA transitions, the natural transition orbitals (NTOs) were analyzed.⁷¹ To estimate the threshold energies for the formation of the radical cations, we computed the (gas-phase) vertical ionization potentials (IPs) of **1**, **2**, and **3** employing the electron propagator theory in the renormalized partial third order approximation (EPT-P3+)⁷² with the Dunning's polarized valence triple- ζ cc-pVTZ basis set.⁷³

The vertical absorption spectra of singlet (spin-restricted) and triplet (spin-unrestricted) **car-1**, **car-2**, and **car-3** were computed at the TD-CAM-B3LYP(+PCM)/6-311+G(2d,p) level. In addition, we tried the single-state multiconfigurational perturbation theory to the second order (CASPT2).⁷⁴ To obtain the CASSCF reference wave functions, in case of **car-1** we used the active space of 10 electrons in 10 orbitals (10,10), which is (4,4) per each benzene ring and (2,2) for correlating the carbene lone pair (the next larger active space would amount to (14,14), which is too expensive). In case of **car-2** and **car-3**, the (8,8) active spaces were used, viz. (6,6) on the benzene ring (i.e. the entire benzene π -system), and (2,2) for the carbene lone pair. The cc-pVTZ basis set was employed for **car-1** and the smaller cc-pVDZ for **car-2** and **car-3**.⁷³ The 10 lowest state-averaged equally weighted CASSCF roots were considered. To mitigate the effects of intruder states, the imaginary level shift of 0.10 au was applied,⁷⁵ which proved beneficial in our previous studies.^{76,77} The oscillator strengths are based on the expectation values of the dipole moment operator (the length representation) between the CASSCF references.⁷⁸ The CASPT2 spectra were computed for the gas-phase; in view of the small dielectric constant of the solvent cyclohexane, this is not expected to introduce major discrepancies relative to the solvated phase. To investigate the intramolecular rearrangements and final products of the singlet **car-2** and **car-3**, the corresponding transition states and reaction activation energies were computed at the DFT(+PCM)/6-311+G(2d,p) level employing several density functionals (see SI). The rate constants for these reactions were estimated in the formalism of the transition state theory (TST) with the Wigner tunneling coefficient (WTC).

The following quantum chemistry codes were used: Gaussian 16, revision C.01⁷⁹ (the PCM-DFT optimizations and harmonic frequencies of the S_0 states and transition states; the EPT-P3+ IPs), OpenMolcas 22.06⁸⁰ (the CASSCF/CASPT2 computations of the vertical spectra of the singlet

and triplet **car-1-3**), and Orca 5.0.3^{81, 82} (the RIJCOSX-DFT(+CPCM) optimizations and harmonic frequencies of the S₁ minima; the ESA spectra; the NTOs). The GaussView 5 program was used for visualizing the NTOs.⁸³

Associated Content

Data Availability Statement The data are available from the corresponding author upon request.

Supporting information contains:

Supporting information contains detailed experimental procedures for the synthesis of known compounds and photochemistry, UV-vis and fluorescence data, fs-TA and LFP data, computational details, copies of ¹H and ¹³C NMR spectra and coordinates of the optimized molecular structures. The Supporting Information is available free of charge on the ACS website.

Acknowledgement

These materials are based on work financed by the Croatian Science Foundation (HrZZ-UIP-05-2017-5831 to SV, HrZZ-IP-2020-02-9932 to IL, HRZZ-IP-2014-09-6312 and HrZZ-IP-2019-04-8008). The authors thank Cornelia Bohne for granting access to the VicPicK-CAMTEC facility for the experiments performed at the University of Victoria.

& Present address:

Zernike Institute for Advanced Materials, University of Groningen, Nijenborgh 4, 9747 AG,
Groningen, the Netherlands

References:

-
- ¹ Hine, J. Carbon Dichloride as an Intermediate in the Basic Hydrolysis of Chloroform. A Mechanism for Substitution Reactions at a Saturated Carbon Atom. *J. Am. Chem. Soc.* **1950**, *72*, 2438-2445.
- ² von Doering, W. E.; Buttery, R. G.; Laughlin, R. G.; Chaudhury, N. Indiscriminate Reaction of Methylene with the Carbon-Hydrogen Bond. *J. Am. Chem. Soc.* **1956**, *78*, 3224-3224.
- ³ Moss, R. A.; Doyle, M. P. *Contemporary Carbene Chemistry*; Wiley, 2014.
- ⁴ Jones, M. Jr.; Moss, R. A. Singlet Carbenes. In *Reactive Intermediate Chemistry*, Wiley; 2004; pp 273-328, and references cited therein.
- ⁵ Tomioka, H. Triplet Carbenes. In *Reactive Intermediate Chemistry*; Wiley, 2004; pp 375-461, and references cited therein.
- ⁶ Bourissou, D.; Guerret, O.; Gabbai, F. P.; Bertrand, G. Stable Carbenes. *Chem. Rev.* **2000**, *100*, 39-91.
- ⁷ de Frémont, P.; Marion, N.; Nolan, S. P. Carbenes: Synthesis, Properties, and Organometallic Chemistry. *Coord. Chem. Rev.* **2009**, *253*, 862-892.
- ⁸ Hopkinson, M. N.; Richter, C.; Schedler, M.; Glorius, F. An Overview of *N*-Heterocyclic Carbenes. *Nature* **2014**, *510*, 485-496.
- ⁹ Platz, M. S. A Perspective on Physical Organic Chemistry. *J. Org. Chem.* **2014**, *79*, 2341-2355.
- ¹⁰ Moss, R. A. Adventures in Reactive Intermediate Chemistry: A Perspective and Retrospective. *J. Org. Chem.* **2017**, *82*, 2307-2318.
- ¹¹ Abdel-Wahab, A.-M. A.; Ahmed, S. A.; Dürr, H. Carbene Formation by Extrusion of Nitrogen. In *CRC Handbook of Photochemistry and Photobiology 2nd Ed.*; CRC Press, 2004.
- ¹² Nakamoto, K.; Ueno, Y. Diazirine-Containing RNA Photo-Cross-Linking Probes for Capturing micro RNA Targets. *J. Org. Chem.* **2014**, *79*, 2463-2472.

-
- ¹³ Holland, J. P.; Gut, M.; Klingler, S.; Fay, R.; Guillou, A. Photochemical Reactions in the Synthesis of Protein-Drug Conjugates. *Chem. Eur. J.* **2020**, *26*, 33-48.
- ¹⁴ Maas, G. New Syntheses of Diazo Compounds. *Angew. Chem. Int. Ed.* **2009**, *48*, 8186-8195.
- ¹⁵ Black, T. H. The Preparation and Reactions of Diazomethane. *Aldrichimica Acta*, **1983**, *16*, 1-22.
- ¹⁶ Johnston, J. N.; Muchalski, H.; Troyer, T. L. To Protonate or Alkylate? Stereoselective Brønsted Acid Catalysis of C-C Bond Formation Using Diazoalkanes. *Angew. Chem. Int. Ed.* **2010**, *49*, 2290-2298.
- ¹⁷ Padwa, A.; Weingarten, M. D. Cascade Processes of Metallo Carbenoids. *Chem. Rev.* **1996**, *96*, 223-269.
- ¹⁸ Gutiérrez, S.; Tomás-Gamasa, M.; Mascareñas, J. L. Exporting Metal-Carbene Chemistry to Live Mammalian Cells: Copper-Catalyzed Intracellular Synthesis of Quinoxalines Enabled by N-H Carbene Insertions. *Angew. Chem. Int. Ed.* **2021**, *60*, 22017.
- ¹⁹ Wang, J.; Burdzinski, G.; Gustafson, T. L.; Platz, M. S. Ultrafast Study of p-Biphenylyldiazoethane. The Chemistry of the Diazo Excited State and the Relaxed Carbene. *J. Am. Chem. Soc.* **2007**, *129*, 2597-2606.
- ²⁰ Yamamoto, N.; Bernardi, F.; Bottoni, A.; Olivucci, M.; Robb, M. A.; Wilsey, S. Mechanism of Carbene Formation from the Excited States of Diazirine and Diazomethane: An MC-SCF Study. *J. Am. Chem. Soc.* **1994**, *116*, 2064-2074.
- ²¹ Arenas, J. F.; Lopez-Tocon, I.; Otero, J. C.; Soto, J. Carbene Formation in Its Lower Singlet State from Photoexcited 3H-Diazirine or Diazomethane. A Combined CASPT2 and ab Initio Direct Dynamics Trajectory Study. *J. Am. Chem. Soc.* **2002**, *124*, 1728-1735.
- ²² Piteša, T.; Alešković, M.; Becker, K.; Basarić, N.; Došlić, N. Photoelimination of Nitrogen from Diazoalkanes: Involvement of Higher Excited Singlet States in the Carbene Formation. *J. Am. Chem. Soc.* **2020**, *142*, 9718-9724.
- ²³ Bogdanova, A.; Popik, V. V. Experimental and Theoretical Investigation of Reversible Interconversion, Thermal Reactions, and Wavelength-Dependent Photochemistry of Diazo Meldrum's Acid and Its Diazirine Isomer, 6,6-Dimethyl-5,7-dioxa-1,2-diaza-spiro[2,5]oct-1-ene-4,8-dione. *J. Am. Chem. Soc.* **2002**, *124*, 1728-1735.
- ²⁴ Nigam, M.; Platz, M. S.; Showalter, B. M.; Toscano, J. P.; Johnson, R.; Abbot, S. C.; Kirchoff, M. M. Generation and Study of Benzylchlorocarbene from a Phenanthrene Precursor. *J. Am. Chem. Soc.* **1998**, *120*, 8055-8059.

-
- ²⁵ Bonneau, R.; Liu, M. T. H.; Kim, K. C.; Goodman, J. L. Rearrangement of Alkylchlorocarbenes: 1,2-H Shift in Free Carbene, Carbene-Olefin Complex, and Excited States of Carbene Precursors. *J. Am. Chem. Soc.* **1996**, *118*, 3829-3837.
- ²⁶ Burdzinski, G.; Wang, J.; Gustafson, T. L.; Platz, M. S. Study of Concerted and Sequential Photochemical Wolff Rearrangement by Femtosecond UV-vis and IR Spectroscopy. *J. Am. Chem. Soc.* **2008**, *130*, 3746-3747.
- ²⁷ Wang, J.; Burdzinski, G.; Kubicki, J.; Platz, M. S. Ultrafast UV-Vis and IR Studies of p-Biphenyl Acetyl and Carbomethoxy Carbenes. *J. Am. Chem. Soc.* **2008**, *130*, 11195-11209
- ²⁸ Burdzinski, G.; Zhang, Y.; Selvaraj, P.; Sliwa, M.; Platz, M. S. Direct Observation of 1,2-Hydrogen Migration in the Excited States of Alkyl Diazo Esters by Ultrafast Time Resolved IR Spectroscopy. *J. Am. Chem. Soc.* **2010**, *132*, 2126-2127.
- ²⁹ Platz, M. S.; Huang, H. Y.; Ford, F.; Toscano, J. Photochemical rearrangements of diazirines and thermal rearrangements of carbenes. *Pure Appl. Chem.* **1997**, *69*, 803-807.
- ³⁰ Motschieder, K.; Gudmundsdottir, A.; Toscano, J. P.; Platz, M.; Garcia-Garibay, M. A. Excited Precursor Reactivity, Fast 1,2-H Shifts, and Diffusion-Controlled Methanol Insertion in 1,2-Diphenylalkylidenes. *J. Org. Chem.* **1999**, *64*, 5139-5147.
- ³¹ Demchenko, A. P.; Tomin, V. I. Chou, P. T. Breaking the Kasha Rule for More Efficient Photochemistry. *Chem. Rev.* **2017**, *117*, 13353-13381.
- ³² Wang, Y.; Sitzmann, E. V.; Novak, F.; Dupuy, C.; Eisenthal, K. B. Reactions of Excited Triplet Diphenylcarbene Studied with Picosecond Lasers. *J. Am. Chem. Soc.* **1982**, *104*, 3238-3239.
- ³³ Casal, H. L.; Sugamori, S. E.; Scaiano, J. C. Study of Carbonyl Oxide Formation in the Reaction of Singlet Oxygen with Diphenyldiazomethane. *J. Am. Chem. Soc.* **1984**, *106*, 7623-7624.
- ³⁴ Sitzmann, E. V.; Langan, J. G.; Eisenthal, K. B. Picosecond Laser Studies of The Effects of Reactants on Intramolecular Energy Relaxation of Diphenylcarbene: Reaction of Diphenylcarbene with Alcohols. *Chem. Phys. Lett.* **1984**, *112*, 111-116.
- ³⁵ Eisenthal, K. B.; Turro, N. J.; Sitzmann, E. V.; Gould, I. R.; Hefferon, G.; Langan J.; Cha, Y. Singlet-Triplet Interconversion of Diphenylmethylene. Energetics, Dynamics and Reactivities of Different Spin States. *Tetrahedron*, **1985**, *41*, 1543-1554.
- ³⁶ Griller, D.; Majewski, M.; McGimpsey, W. G.; Nazran, A. S., Scaiano, J. C. Reaction of Diphenylcarbene with Diphenyldiazomethane. *J. Org. Chem.* **1988**, *53*, 1550-1553.

-
- ³⁷ Wolfgang Kirmse, W.; Kilian, J. Carbenes and the O-H Bond: Spectroscopic Evidence for Protonation of Diarylcarbenes to Give Diarylcarbenium Ions. *J. Am. Chem. Soc.* **1990**, *112*, 6399-6400.
- ³⁸ Portella-Oberli, M. T.; Jeannin, C.; Soep, B.; Zerza, G.; Chergui, M. Femtosecond study of the rise and decay of carbenes in solution. *Chem. Phys. Lett.* **1998**, *296*, 323-328.
- ³⁹ Peon, J.; Polshakov, D.; Kohler, B. Solvent Reorganization Controls the Rate of Proton Transfer from Neat Alcohol Solvents to Singlet Diphenylcarbene. *J. Am. Chem. Soc.* **2002**, *124*, 6428-6438.
- ⁴⁰ Costa, P.; Sander, W. Hydrogen Bonding Switches the Spin State of Diphenylcarbene from Triplet to Singlet. *Angew. Chem. Int. Ed.* **2014**, *53*, 5122-5125.
- ⁴¹ Costa, P.; Fernandez-Oliva, M.; Sanchez-Garcia, E.; Sander, W. The Highly Reactive Benzhydryl Cation Isolated and Stabilized in Water Ice. *J. Am. Chem. Soc.* **2014**, *136*, 15625-15630.
- ⁴² Knorr, J.; Sokkar, P.; Schott, S.; Costa, P.; Thiel, W.; Sander, W.; Sanchez-Garcia, E.; Nuernberger, P. Competitive solvent-molecule interactions govern primary processes of diphenylcarbene in solvent mixtures. *Nature Commun.* **2016**, *7*, 12968. DOI: 10.1038/ncomms12968
- ⁴³ Knorr, J.; Sokkar, P.; Costa, P.; Sander, W.; Sanchez-Garcia, E.; Nuernberger, P. How Protic Solvents Determine the Reaction Mechanisms of Diphenylcarbene in Solution. *J. Org. Chem.* **2019**, *84*, 11450-11457.
- ⁴⁴ Ohno, M.; Itoh, M.; Umeda, M.; Furuta, R.; Kondo, K.; Eguchi, S. Conjugatively Stabilized Bridgehead Olefins: Formation and Reaction of Remarkably Stable Homoadamant-3-enes Substituted with Phenyl and Methoxycarbonyl Groups. *J. Am. Chem. Soc.* **1996**, *118*, 7075-7082.
- ⁴⁵ Fernández, I.; Frenking, G. Direct Estimate of the Strength of Conjugation and Hyperconjugation by the Energy Decomposition Analysis Method. *Chem. Eur. J.* **2006**, *12*, 3617-3629.
- ⁴⁶ Šumanovac, T.; Alešković, M.; Šekutor, M.; Matković, M.; Baron, T.; Mlinarić-Majerski, K.; Bohne, C.; Basarić, N. Photoelimination of Nitrogen from Diazirines: Spectroscopic Study and Supramolecular Control. *Photochem. Photobiol. Sci.* **2019**, *18*, 1806-1822.
- ⁴⁷ Hatchard, C. G.; Parker, C. A. A new sensitive chemical actinometer – II. Potassium ferrioxalate as a standard chemical actinometer. *Proc. Roy. Soc. A* **1956**, *235*, 518-336.

-
- ⁴⁸ Kuhn, H. J.; Braslavsky, S. E.; Schmidt, R. Chemical Actinometry. *Pure Appl. Chem.* **2004**, *76*, 2105-2146.
- ⁴⁹ Gerbig, D.; Ley, D. Computational Methods for Contemporary Carbene Chemistry. *WIREs Comput. Mol. Sci.* **2013**, *3*, 242-272.
- ⁵⁰ Snellenburg, J. J.; Liptenok, S.P.; Seger, R.; Mullen, K.M.; van Stokkum, I.H. Glotaran: a Java-Based Graphical User Interface for the R Package TIMP. *J. Stat. Softw.* **2012**, *49*, 1-22.
- ⁵¹ Hirai, K.; Tomioka, H.; Okazaki, T.; Tokunaga, K.; Kitagawa, T.; Takeuchi, K. Laser Flash Photolysis of 3-noradamantyl(phenyl)diazomethane: Generation, Detection and Kinetics of 2-phenyladamantene. *J. Phys. Org. Chem.* **1999**, *12*, 165-169.
- ⁵² Lee Tae, E.; Zhu, Z.; Platz, M. S. A Matrix Isolation, Laser Flash Photolysis, and Computational Study of Adamantene. *J. Phys. Chem. A.* **2001**, *105*, 3803-3807.
- ⁵³ Montalti, M.; Credi, A.; Prodi, L.; Gandolfi, M. T. *Handbook of Photochemistry*; CRC press, 2006.
- ⁵⁴ Nikšić-Franjić, I.; Ljubić, I. Comparing the Performances of Various Density Functionals for Modelling the Mechanisms and Kinetics of Bimolecular Free Radical reactions in Aqueous Solution. *Phys. Chem. Chem. Phys.* **2019**, *21*, 23425-23440.
- ⁵⁵ de Souza, B.; Farias, G.; Neese, F.; Izsak, R. Predicting Phosphorescence Rates of Light Organic Molecules Using Time-Dependent Density Functional Theory and the Path Integral Approach to Dynamics. *J. Chem. Theory Comput.* **2019**, *15*, 1896-1906.
- ⁵⁶ Forjan, M.; Zgrablić, G.; Vdović, S.; Šekutor, M.; Basarić, N.; Kabacinski, P.; Nazari Haghighi Pashaki, M.; Frey, H.-M.; Cannizzo, A.; Cerullo, G. Photogeneration of Quinone Methide from Adamantylphenol in an Ultrafast Non-adiabatic Dehydration Reaction. *Phys. Chem. Chem. Phys.* **2022**, *24*, 4384-4393.
- ⁵⁷ Liao, Y.; Bohne, C. Alcohol Effect on Equilibrium Constants and Dissociation Dynamics of Xanthone-Cyclodextrin Complexes. *J. Phys. Chem.* **1996**, *100*, 734-743.
- ⁵⁸ Pace, T. C. S.; Bohne, C. Temperature Effects on Xanthone- β -Cyclodextrin Binding Dynamics. *Can. J. Chem.*, **2011**, *89*, 395-401.
- ⁵⁹ Yanai, T.; Tew, D. P.; Handy, N. C. A New Hybrid Exchange–Correlation Functional Using the Coulomb-Attenuating Method (CAM-B3LYP). *Chem. Phys. Lett.* **2004**, *393*, 51-57.
- ⁶⁰ Loos, P.-F.; Comin, M.; Blase, X.; Jacquemin, D. Reference Energies for Intramolecular Charge-Transfer Excitations. *J. Chem. Theory Comput.* **2021**, *17*, 3666-3686.

-
- ⁶¹ Weigend, F.; Ahlrichs, R. Balanced Basis Sets of Split Valence, Triple Zeta Valence and Quadruple Zeta Valence Quality for H to Rn: Design and Assessment of Accuracy. *Phys. Chem. Chem. Phys.* **2005**, *7*, 3297-3305.
- ⁶² Zheng, J.; Xu, X.; Truhlar, D. G. Minimally Augmented Karlsruhe Basis Sets. *Theor. Chem. Acc.* **2011**, *128*, 295-305.
- ⁶³ Neese, F.; Wennmohs, F.; Hansen, A.; Becker, U. Efficient, Approximate and Parallel Hartree–Fock and Hybrid DFT Calculations. A ‘Chain-of-Spheres’ Algorithm for the Hartree–Fock Exchange. *Chem. Phys.* **2009**, *356*, 98-109.
- ⁶⁴ Weigend, F. Accurate Coulomb-Fitting Basis Sets for H to Rn. *Phys. Chem. Chem. Phys.* **2006**, *8*, 1057-1065.
- ⁶⁵ Neese, F. An Improvement of the Resolution of the Identity Approximation for the Formation of the Coulomb Matrix. *J. Comput. Chem.* **2003**, *24*, 1740-1747.
- ⁶⁶ Mennucci, B. Polarizable Continuum Model. *WIREs Comput. Mol. Sci.* **2012**, *2*, 386-404.
- ⁶⁷ Barone, V.; Cossi, M. Quantum Calculation of Molecular Energies and Energy Gradients in Solution by a Conductor Solvent Model. *J. Phys. Chem. A* **1998**, *102*, 1995-2001.
- ⁶⁸ Scalmani, G.; Frisch, M. J. Continuous Surface Charge Polarizable Continuum Models of Solvation. I. General formalism. *J. Chem. Phys.* **2010**, *132*, 114110.
- ⁶⁹ Grimme, S.; Ehrlich, S.; Goerigk, L. Effect of the Damping Function in Dispersion Corrected Density Functional Theory. *J. Comp. Chem.* **2011**, *32*, 1456-65.
- ⁷⁰ Hirata, S.; Head-Gordon, M. Time-Dependent Density Functional theory within the Tamm–Dancoff Approximation. *Chem. Phys. Lett.* **1999**, *314*, 291-299.
- ⁷¹ Martin, R. L. Natural Transition Orbitals. *J. Chem. Phys.* **2003**, *118*, 4775-4777.
- ⁷² Ortiz, J. V. An Efficient, Renormalized Self-Energy for Calculating the Electron Binding Energies of Closed-Shell Molecules and Anions. *Int. J. Quantum Chem.* **2005**, *105*, 803-808.
- ⁷³ Dunning, T. H. Jr. Gaussian Basis Sets for Use in Correlated Molecular Calculations. I. The Atoms Boron through Neon and Hydrogen. *J. Chem. Phys.* **1989**, *90*, 1007-1023.
- ⁷⁴ Andersson, K.; Malmqvist, P.-Å.; Roos, B. O. Second-Order Perturbation Theory with a Complete Active Space Self-Consistent Field Reference Function. *J. Chem. Phys.* **1992**, *96*, 1218-1226.

-
- ⁷⁵ Forsberg, N.; Malmqvist, P.-Å. Multiconfiguration Perturbation Theory with Imaginary Level Shift. *Chem. Phys. Lett.* **1997**, *274*, 196-204.
- ⁷⁶ Ljubić, I.; Sabljic, A. CASSCF/CASPT2 and TD-DFT Study of Valence and Rydberg Electronic Transitions in Fluorene, Carbazole, Dibenzofuran, and Dibenzothiophene. *J. Phys. Chem. A* **2011**, *115*, 4840-4850.
- ⁷⁷ Ljubić, I.; Sabljic, A. Theoretical Study of Structure, Vibrational Frequencies, and Electronic Spectra of Polychlorinated Dibenzo-*p*-dioxins. *J. Phys. Chem. A* **2006**, *110*, 4524-4534.
- ⁷⁸ Malmqvist, P.-Å.; Roos, B. O. The CASSCF State Interaction Method, *Chem. Phys. Lett.* **1989**, *155*, 189-194.
- ⁷⁹ Frisch, M. J. et al., Gaussian 16, Revision C.01, Gaussian, Inc., Wallingford CT, 2019.
- ⁸⁰ Galván, I. F. et al., OpenMolcas: From Source Code to Insight, *J. Chem. Theory Comput.* **2019**, *15*, 5925-5964.
- ⁸¹ Neese, F., The ORCA Program System, *WIREs Comput. Mol. Sci.*, **2012**, *2*, 73-78.
- ⁸² Neese, F. Software Update: The ORCA Program System, Version 4.0. Wiley Interdisciplinary Rev.: Compt. Mol. Sci. **2017**, *8*, e1327.
- ⁸³ Dennington, R.; Keith, T. A.; Millam, J. M., GaussView, Version 5, Semichem Inc., Shawnee Mission, KS, 2009.